Nuclear Instruments and Methods in Physics Research A 624 (2010) 699–707

Contents lists available at ScienceDirect

Nuclear Instruments and Methods in Physics Research A

journal homepage: www.elsevier.com/locate/nima

Neutron production with a pyroelectric double-crystal assembly without nano-tip

W. Tornow [a,*], W. Corse [a], S. Crimi [b,1], J. Fox [a]

[a] Department of Physics, Duke University and Triangle Universities Nuclear Laboratory, Durham, NC 27708-0308, USA
[b] Harriet L. Wilkes Honors College, Florida Atlantic University, Jupiter, FL 33458, USA

ARTICLE INFO

Article history:
Received 27 May 2010
Received in revised form
20 September 2010
Accepted 24 September 2010
Available online 8 October 2010

Keywords:
Pyroelectric crystals
Nuclear fusion
Neutrons

ABSTRACT

Two cylindrical $LiTaO_3$ crystals facing each other's deuterated circular face were exposed to deuterium gas at an ambient pressure of a few mTorr. With a distance of about 4 cm between the z^+ and z^- cut crystal faces, neutrons were produced via the $^2H(d,n)^3He$ fusion reaction upon the heating and cooling of the crystals. The 2.5 MeV neutrons were detected with organic liquid scintillation detectors equipped with neutron-gamma pulse-shape discrimination electronics to reject pulses generated by the intense X-ray flux. During the cooling phase of naked crystals, deuterium ion-beam (D_2^+) energies of up to 400 keV were obtained as deduced from the associated electron bremsstrahlung end-point energy. The highest electron-beam energy observed during the heating phase was 360 keV. With a layer of deuterated polyethylene evaporated on the front face of the crystals, the maximal energies were about 10% lower. In contrast to earlier studies, an electric-field enhancing nano-tip was not employed. Neutron yields up to 500 per thermal cycle were observed, resulting in a total neutron production yield of about 1.6×10^4 neutrons per thermal cycle. Our approach has the potential of being substantially improved by reducing the frequency of the discharges we are currently experiencing with our geometry, which was not designed for the unprecedented high potentials produced in the present work.

1. Introduction

Since the ground-breaking work of the UCLA [1] and RPI [2] groups in 2005, the production of neutrons with pyroelectric crystals has been the subject of considerable interest, but also of some skepticism. The lack of reproducibility may be one of the reasons why the UCLA group has not published any further papers after its pioneering article in Nature [1]. However, they teamed up with scientists from Livermore National Laboratory and reported unprecedented high neutron yields [3]. In this work the liquid scintillator neutron detector was replaced by an array of ^3He filled proportional counters, which are less sensitive to the intense X-ray flux associated with pyroelectric fusion experiments. This change in the neutron detection technique may be an indication of problems associated with the neutron detection in the original work, as was speculated in Ref. [4]. To account for the neutron yield of 8.5×10^4 per thermal cycle in the original UCLA work and of 1.9×10^5 in the follow-up work with the LLNL group of Tang et al. [3], the deuterium ion beam had to consist predominately of D^+ ions and not of D_2^+ ions. However, there is no independent experimental proof that this was in fact the case. A more recent study by the RPI group indicates that the deuterium ion beams generated in pyroelectric crystal experiments most likely consist of only D_2^+ ions [5]. As a result, a 100 kV acceleration potential, which is typical for single pyroelectric crystals, can only create 50 keV deuterons. Due to the associated factor of a 3.5 decrease in $^2H(d,n)^3He$ cross-section compared to 100 keV deuterons, it seems very difficult to account for the neutron yield reported in Refs. [1,3]. The LLNL group did not publish further experimental results with the technique described in Ref. [3], but instead resorted to a spark ion source for generating deuterium ions [6], which were subsequently accelerated by a pyroelectric crystal. Because the LLNL group no longer used the technique described in Ref. [3], we assume that further improvements in neutron yield using this method are unlikely.

The lack of reproducibility may be associated with the nano-tip attached to the pyroelectric crystal to enhance the electric-field strength and/or with insufficient experience in detecting 2.5 MeV neutrons in the presence of a strong X-ray background. The pile-up of X-ray events can mimic the pulse shape of neutron induced pulses [4] in most neutron detectors and therefore, may result in a flawed neutron yield determination.

The RPI group continues to publish results on their neutron production work. With their double-crystal arrangement they double the acceleration potential over that achieved by the UCLA

* Corresponding author.
E-mail address: tornow@tunl.duke.edu (W. Tornow).
[1] Summer 2009 NSF REU student at TUNL.

0168-9002/$ - see front matter © 2010 Elsevier B.V. All rights reserved.
doi:10.1016/j.nima.2010.09.139

and LLNL groups, resulting in a factor of slightly more than two increases in fusion cross-section. Like the UCLA and LLNL groups, they also use an electric-field enhancing nano-tip attached to one of the two crystals, while the front face of the second crystal is coated with deuterated polystyrene or polyethylene. However, more recently, the neutron yield reported by the RPI group appears to have a downward trend. While in 2005 [2] and 2007 [7] the group published a maximum yield of 1×10^4 and 5.9×10^4 neutrons per thermal cycle, respectively, the most recent work refers to "only" 1.1×10^4 neutrons per thermal cycle [8,9]. Surprisingly, in the latter work the highest neutron yield was obtained at an ambient deuterium gas pressure of 26 mTorr. Therefore, a measurable amount of neutrons would have been produced in the deuterium gas in addition to the neutrons produced in the deuterated target. Neutron production with a pyroelectric crystal in deuterium gas and without a deuterated target was first reported in Ref. [4].

In the present work we removed the two main sources of potential irreproducibility, the nano-tip and any issues related to the detection of 2.5 MeV neutrons in the presence of intense and high-energy bremsstrahlung X rays. We adopted the double-crystal scheme of the RPI group, and for the first time reported on the production of neutrons during both the heating and cooling phases of the crystal assembly.

2. Experimental approach

Following our recent work [12] where acceleration potentials of up to 310 kV have been achieved with a single pyroelectric crystal, we assembled two 2.5 cm long and 2.5 cm diameter $LiTaO_3$ crystals in a double-crystal arrangement similar to the one pioneered by the RPI group [2]. Fig. 1 shows a cartoon of the double-crystal assembly. The electric heater/cooler devices were glued with non-conductive epoxy to vertical copper plates with a thin layer of heat-sink paste between them. Without the heat-sink paste it was impossible to cool the crystals from 130 °C down to 0 °C. The copper disks and the $LiTaO_3$ crystals were also held in place with non-conductive epoxy. Furthermore, a thermocouple was attached to the heater/cooler device of the crystal shown on the left side in Fig. 1. This z-cut crystal was mounted with its z^+ side facing to the right to provide a positive polarization charge during cooling, while at the same time the z^- side of the z-cut crystal shown on the right side provided a negative polarization charge. During the heating phase of the crystals the two polarization charges are inverted.

Because we had limited experience with double-crystal arrangements, we conditioned the two crystals individually and without deuterated polyethylene evaporated on their front face. Using the apparatus, geometry and procedure described in Ref. [12], we achieved maximum positive deuterium ion energies of up to 315 and 325 kV, respectively, for the two individual crystals during the cooling phase (130–0 °C), while the z^+ face was exposed to deuterium gas of 6 mTorr. The maximum electron energies observed during the heating phase (room temperature to 130 °C) were about 220 kV. The reduced potential obtained during the heating phase can be explained partially by the smaller change in temperature ΔT. Theoretically, the achievable potential is proportional to ΔT. After assembling the two-crystal arrangement, the conditioning and optimization process was repeated, again without deuterated polyethylene on the crystal faces. Because the two-crystal arrangement precludes us from measuring the electron and ion energies directly, we used a high-purity germanium (HPGe) planar detector positioned outside of the chamber, as shown in Fig. 2. In order to reduce the rate in this detector, it was shielded by

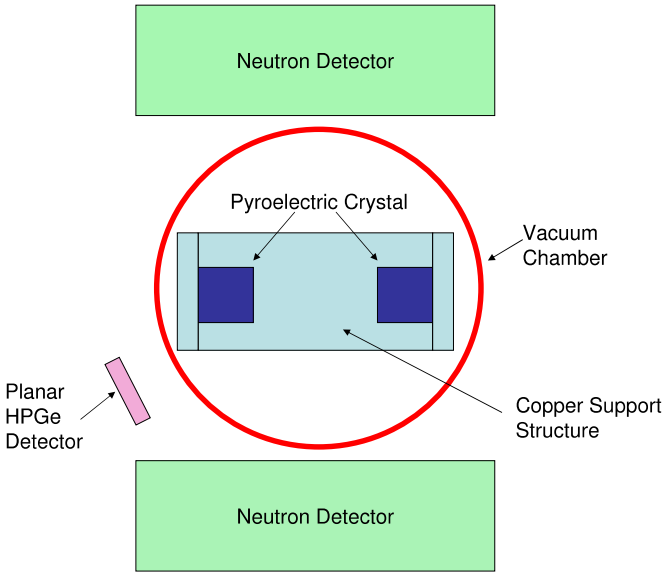

Fig. 2. Cartoon of top view of chamber containing the double-crystal arrangement. Also shown are the two neutron detectors and the HPGe detector for X-ray detection, all positioned in the horizontal plane. For a side view see Fig. 4.

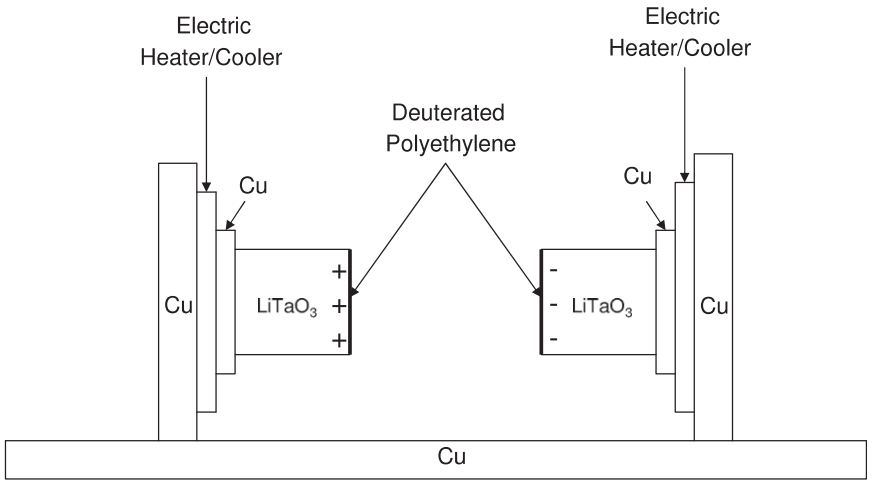

Fig. 1. Cartoon of double-crystal arrangement. The polarity of the polarization charges shown is for the cooling phase. The polarity is reversed during the heating phase of the crystals.

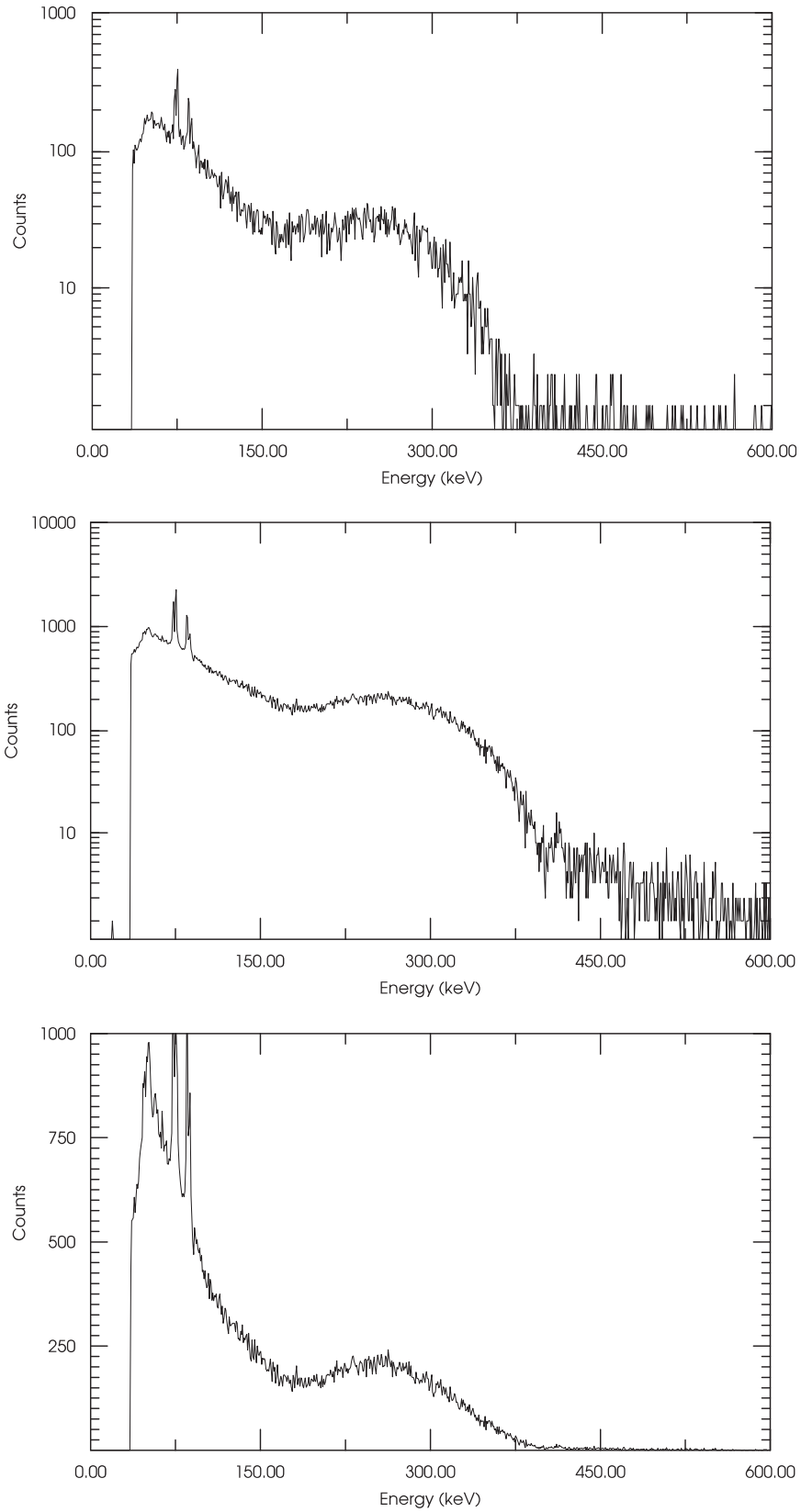

Fig. 3. (Top panel) Bremsstrahlung spectrum obtained with HPGe detector during heating phase of double-crystal arrangement. Note the logarithmic scale for the number of counts on the vertical axis. The bremsstrahlung end-point energy is slightly above 350 keV. The peaks at lower energies are due to Pb K_α and K_β X-rays. (Center panel) Same as above, but here the bremsstrahlung spectrum was obtained during the cooling phase. The end-point energy is 400 keV after correcting for pile-up events. (Bottom panel) Same as center panel, but using a linear scale for the number of counts, which provides a more accurate visual determination of the X-ray end-point energy.

a $\frac{1}{4}$–in. thick disk of lead to guarantee a reliable determination of the electron bremsstrahlung end-point energy. As can be seen from Fig. 3, the highest energies observed were about 360 and 400 keV during the heating and cooling phases of the crystals, respectively. The separation between the two crystal faces was 3.9 cm, and the deuterium gas pressure was 3.5 mTorr. The heating phase from room temperature to 130 °C lasted 30 min, while the optimal cooling phase from 130 to 0 °C was found to be 20 min. During the heating and cooling phases we typically experienced two and three discharges, respectively (details are given in Section 3).

Discharges occur once the electrostatic potential between the two crystals or between the crystals and their surroundings exceeds the break-down potential of the ionized gas. Ultimately, discharges were the limiting factors in reaching higher potentials than the one reported in this work. We increased the separation between the crystals from 3.9 to 5.9 cm, without achieving higher acceleration potentials. This finding indicates that for our geometry the discharges most likely take place between the crystals and the bottom copper base plate, which is located as close as 1.7 cm from the rim of the crystals. Unfortunately, our chamber had no windows to visually inspect the crystals during the heating and cooling phases in order to localize any discharge tracks.

However, inspecting the crystal assembly after operating it for about 100 runs, we noticed quite a number of small craters forming a circle around the crystal on the copper disk at the bottom of each crystal. This clearly shows that discharges also occurred between the two oppositely charged surfaces of the crystal. Discharge currents were not measured. Some of the discharges were so violent that they were not only clearly audible, but also disabled the National Instruments data-acquisition cards (DAQs) [10] used in our LabVIEW-based [11] system to operate and control the crystals, although the DAQs were protected by additional electronic circuitry. In a few cases our data-acquisition computer also got disabled and had to be rebooted.

Identical to the procedure used in our single-crystal studies [12], the electron and positive ion currents were collected from an insulated aluminum disk placed above the two crystals (see Fig. 4). Of course, this measurement does not provide any meaningful determination of the actual current between the two crystals.

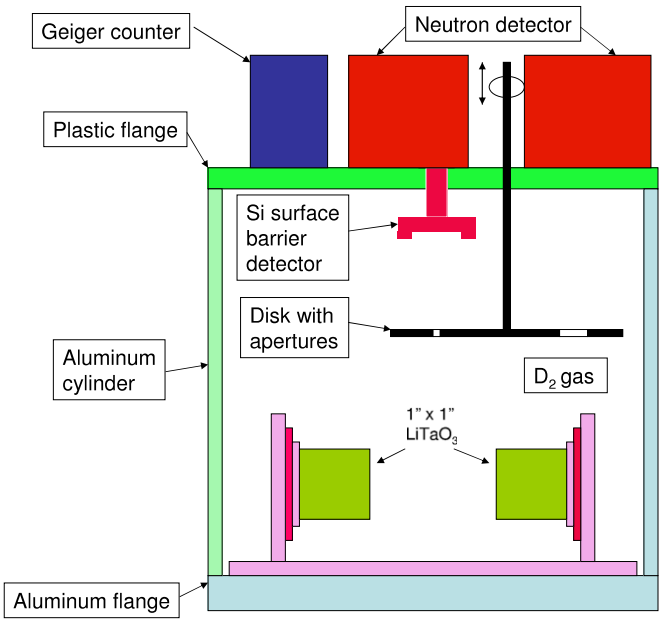

Fig. 4. Cartoon of side view of chamber containing the double-crystal arrangement. The two neutron detectors and the end-window Geiger counter placed on top of the chamber are also shown. The disk above the crystals is used to measure the electron and positive ion currents.

Fig. 5. Photograph of the actual experimental setup showing the chamber containing the double-crystal arrangement, the two large neutron detectors (surrounded by cylinders made of lead) and the HPGe X-ray detector (with a lead attenuator placed in front of the detector) positioned in the horizontal plane and the two small neutron detectors (placed in cups made of lead) and the end-window Geiger counter on top of the chamber.

Finally, we evaporated 0.3 mg/cm^2 of deuterated (99.3%) polyethylene on the crystal faces and afterward reassembled the two-crystal arrangement with its 3.9 cm separation between the crystals. Two 5-in. diameter and 2-in. thick neutron detectors (filled with Bicron 501A [13] liquid scintillator fluid) were positioned on opposite sides of the chamber, as indicated in Fig. 2. They were encased by cylinders made of lead with 1.25-cm thick front face and 1.25-cm wall thickness to provide sufficient X-ray attenuation for reliable neutron detection. Because the lid of our chamber contained the feedthrough for a rotating wheel and the connector for the Si surface-barrier detector used to determine electron and positive ion energies for our standard single-crystal setup [12], it was not possible to position an identical neutron detector on top of the chamber. Instead, we placed two small 2-in. $\times$ 2-in. liquid scintillator detectors (Bicron 501A), again encased by lead cylinders, on top of the chamber (see Fig. 4). Fig. 5 shows a photograph of our experimental setup. All four neutron detectors have excellent neutron-gamma pulse-shape discrimination properties and were connected to an MPD-4 module [14] which provided an amplified pulse-height spectrum and a pulse-shape spectrum with clear separation between γ–ray/ X-ray and neutron induced events. Our neutron detectors were previously used in a variety of experiments at TUNL.

3. Results

Fig. 6 shows a typical pulse-shape spectrum obtained with a discriminator threshold set to one-fourth times the Compton edge of ^{137}Cs γ–rays, i.e., 120 keV. This electron-energy threshold corresponds to about 450 keV neutron energy for the scintillator type used in the present work. The maximum neutron energy expected from the ^{2}H(d,n)^{3}He reaction is about 2.5 MeV at the angular position of our neutron detectors. Our four neutron detectors were gain matched and they have a well-known neutron detection efficiency [15]. In Fig. 6 the vertical axis represents the pulse height, while the horizontal axis provides the distinction between γ–ray/X – ray events and neutron induced

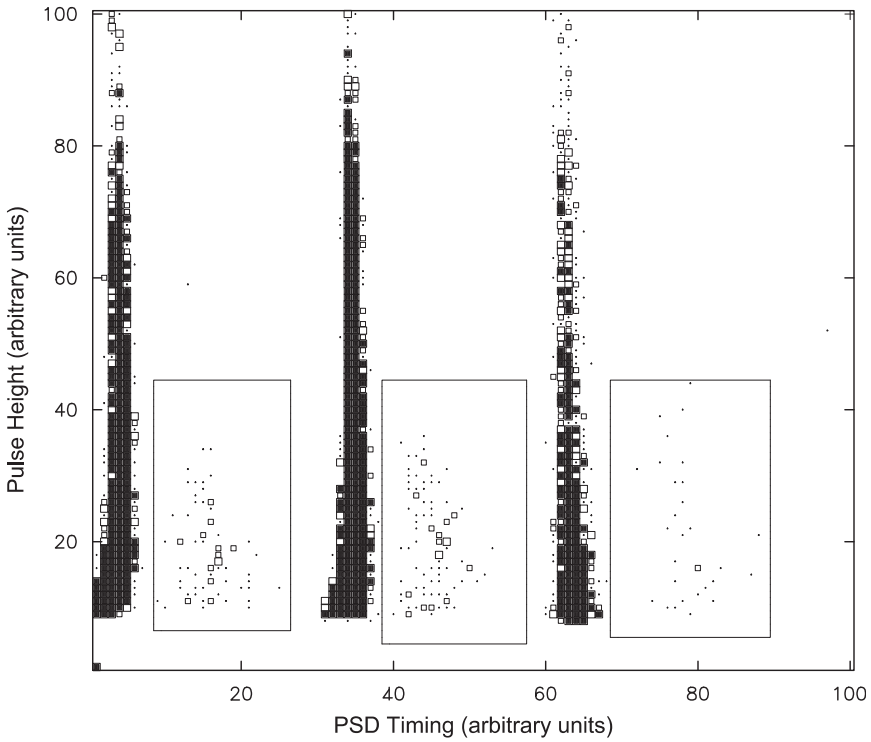

Fig. 6. Two-dimensional spectra of pulse shape versus pulse height for our neutron detectors. The horizontal axis shows the zero-crossing time of X-ray and room-background γ−ray induced pulses (strong vertical bands) and neutron induced pulses (surrounded by rectangles) for the two 5-in. $\times$ 2-in. Bicron 501A neutron detectors (left and center spectrum, respectively) and the two 2-in. $\times$ 2-in. Bicron 501A neutron detectors added together (right spectrum). The vertical axis displays the pulse height.

events. The events located inside the rectangular gate of Fig. 6 are almost exclusively due to the neutrons of interest, while the band to the left, which extends to larger pulse heights, is due to room-background γ−rays. The few events seen above the gate at larger pulse heights are part of the natural neutron background, which of course extends to lower pulse heights as well.

When we operated the double-crystal setup with deuterated polyethylene evaporated onto the front face of both crystals for the first time, we experienced unexpected difficulties in reproducing the high potentials observed earlier without deuterated polyethylene. Even after considerable time was spent with conditioning, we only occasionally recorded bremsstrahlung X-ray energies above 350 keV due to repeated and premature discharges. Nevertheless, the observed neutron yield was quite reproducible, a feature which has plagued some of the previous studies referred to in Section 1. In the new field of pyrofusion, run-to-run reproducibility within a factor of 4 or so is a substantial improvement considering the many parameters involved which have not been studied and characterized yet to sufficient accuracy.

In Fig. 7 we present the measured neutron yield per minute of our four detectors added together and recorded during the cooling phase between discharges as a function of deuterium gas pressure. The maximum neutron yield of about 100 neutrons per min was obtained at deuterium gas pressures centered at the relatively large value of 12 mTorr. Here, the natural neutron background of 5.5 neutrons per minute was already subtracted. We used our standard cooling times of 20 min covering the temperature range from 130 to 0 °C. Surprisingly, such a well-defined pressure dependence as depicted in Fig. 7 was not obtained for the heating phase employing our standard heating time of 30 min, and alternatively 20 min (from room temperature to 130 °C). In these cases, the neutron yield was almost independent of pressure in the pressure range between 2 and 12 mTorr. The results presented in the following were all obtained with a deuterium gas pressure between 10 and 12 mTorr.

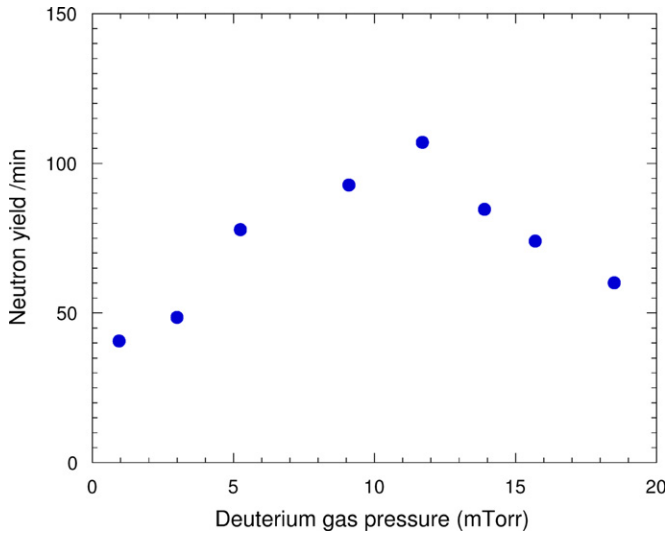

Fig. 7. Neutron yield (per minute) dependence on deuterium gas pressure.

The solid histogram in Fig. 8 shows the measured total neutron yield per thermal cycle as a function of run number, again adding up the yields recorded with our four neutron detectors after background subtraction. Here, the total neutron yield per thermal cycle refers to the yields obtained during the heating and cooling phases of the crystals. The average neutron yield is about 275 neutrons per thermal cycle, with a maximum yield as high as almost 500 neutrons per cycle. For comparison, the dashed histogram shows the associated neutron yield obtained during

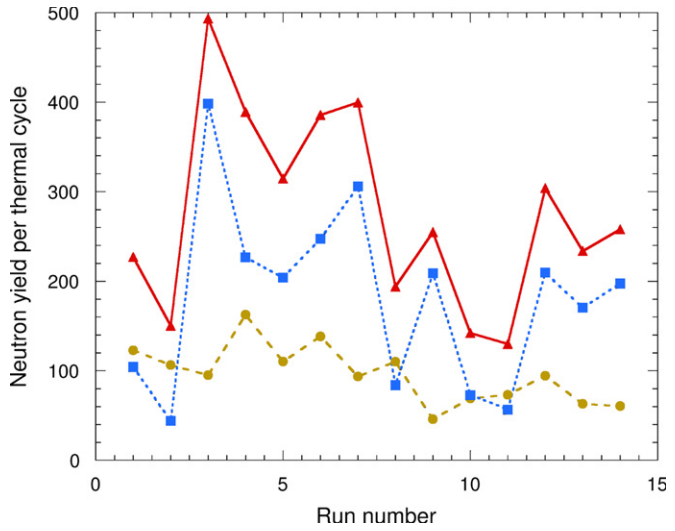

Fig. 8. Neutron yield per thermal cycle during heating phase (dots), cooling phase (squares) and total neutron yield (triangles) for 14 consecutive runs. The natural background yield is subtracted.

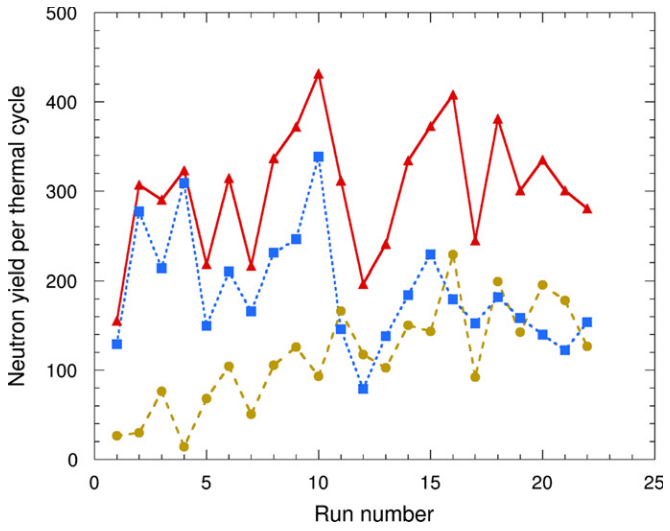

Fig. 9. Same as Fig. 8, but with thicker deuterated polyethylene layers evaporated on the two crystal surfaces and for 22 runs.

the heating phase only, while the dotted histogram displays the neutron yield during the cooling phase. First, we notice that during the cooling phase the neutron yield is on the average a factor of 1.9 larger than found during the heating phase. Second, there is an indication that the neutron yield during heating degraded as a function of run number. Although the visual inspection of the deuterated target layer evaporated on the left crystal shown in Fig. 1 (the one that produces neutrons during the heating phase) did not indicate any potential deterioration, we evaporated new layers of deuterated polyethylene on both crystal faces, this time increasing the thickness to 1.5 mg/cm^2, which is a factor of five thicker than the previous target thickness and about a factor of 10 thicker than needed to stop 400 keV D_2^+ ions. Here, the hope was that such a drastic change in target thickness would also give us some information whether there is a correlation between polyethylene thickness and discharges.

The neutron yield per thermal cycle as a function of run number obtained with the new deuterated polyethylene targets is shown in Fig. 9. Compared to Fig. 8, the average total neutron yield is increased by 10% to about 300 neutrons per thermal cycle, and the yield observed during heating now shows a positive slope. Again, the neutron yield is larger during the cooling phase, but this time only by a factor of 1.6. However, overall there is no substantial difference between the two sets of runs, indicating that there is no factor of two or so of improvement in neutron yield achievable with our present experimental setup, and using our present LabVIEW-controlled operating procedure.

After the end of this run cycle it was noticed that the exposed rim area of each crystal showed a reduction in thickness of the deuterated polyethylene layer, and small flakes of deuterated polyethylene were found on the copper base plate. Apparently, the frequent discharges caused the deuterated polyethylene to "sputter" off the crystals. This observation may in fact be an explanation for the decline in neutron yield found with the thinner layer of deuterated polyethylene shown in Fig. 8.

Fig. 10 shows the X-ray radiation (R) levels recorded with an end-window Geiger counter placed on top of our chamber, the current (I) collected on an insulated disk located above the two-crystal arrangement (see Fig. 4), the temperature (T), and the deuterium pressure (P) as a function of time for run #3 of Fig. 8. It clearly shows how the radiation level tracks the current reading, but more importantly, it also gives a good impression of how

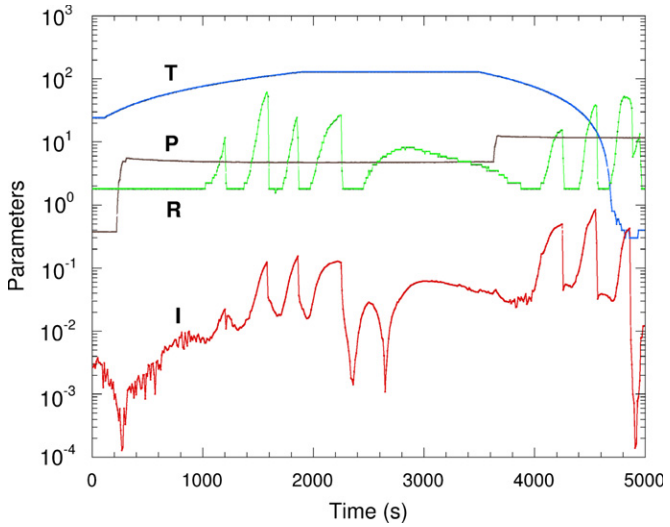

Fig. 10. Temperature (T) in °C, deuterium gas pressure (P) in mTorr, radiation (R) in mrem/h (measured with Geiger counter), and electron/ion current (I) in nA (from top to bottom) during a full thermal cycle as a function of time. Note the logarithmic scale for these parameters. Neutrons are produced when both the radiation and current reading are high. The abrupt declines in radiation and current are due to discharges. The maximum temperature of 130 °C was reached after about 1900 s, while the cooling phase started just before 3600 s. Note that the polarity of the current changed from negative to positive at about 2600 s. Neutrons were not only produced when the radiation and current readings reached high values (three times during the heating phase and three times during the cooling phase, respectively), but also continuously between 2500 and 3500 s, but in the latter case the average neutron yield was very low. See text for details.

much time is wasted recovering from repeated discharges during a complete thermal cycle. A discharge neutralizes the polarization charges on the crystal surface(s) and a considerable change in temperature is required to achieve the potential needed for neutron production again. Eventually, the crystal temperature is equalized and a charge build-up is not possible anymore.

As can be seen from the radiation and current readings of Fig. 10, the first discharge occurred at about $t=1200$ s when the temperature reading of the thermocouple was about 90 °C. At this time the bremsstrahlung end-point energy was about 230 keV and

neutrons were not observed yet. The second discharge took place at about $t=1600$ s when the temperature reading was 112 °C. At this point, the maximal bremsstrahlung end-point energy was about 275 keV and neutrons were produced during a 2.5-min time interval just before the discharge. The crystal(s) discharged a third time before the set temperature of 130 °C was reached, but the potential was not high enough to produce a measurable neutron yield above the background. Because the actual temperature of the crystals lags behind the thermocouple reading recorded at the heater/cooler device, a sizable potential is set up again. The fourth discharge happened at about $t=2300$ s, and neutrons were observed during a 3-min time interval. After this discharge the potential rose only to modest values, thus preventing any further discharges, while the heater/cooler temperature remained constant at 130 °C. During this 16-min stretch neutrons were produced continuously, but at the very low rate of about 3 neutrons per minute above the background. Note that at $t=2600$ s the polarity of the current changed from positive to negative values. At about $t=3500$ s the cool-down process was initiated and shortly thereafter the deuterium gas pressure was increased from 4.8 to 12 mTorr. Near $t=4250$ s the first discharge took place during the cooling phase. The associated temperature reading was 34 °C. Note the increased current compared to the heating phase. Therefore, neutrons were produced already before this discharge within a 2.5-min time interval, although the bremsstrahlung end-point energy was only about 200 keV. Shortly thereafter the current and bremsstrahlung end-point energy increased rapidly and approached 0.8 nA and 300 keV, respectively, resulting in a relatively high neutron yield. After this discharge the current peaked again, but at a lower level. However, due to the higher positive ion energy of about 350 keV, the recorded neutron yield was higher than that obtained before the previous discharge. The temperature at the time of the discharge was 0.3 °C, but this temperature could not be maintained at the 0 °C set value, because the violent spark associated with the last discharge caused our LabVIEW program to "freeze", and as a result, the controlled continuation of this run was not possible anymore.

Summarizing Fig. 10 we note that there are three separate neutron production phases:

(i) The first phase takes place during the heating process of the crystals, extending somewhat into the regime of maximal thermocouple reading (130 °C).
(ii) The second phase occurs during the major part of the constant temperature regime (130 °C).
(iii) The third phase proceeds during the cooling phase, extending into the regime of minimal thermocouple reading (0 °C).

The second neutron production phase normally lasts more than 10 min, and it is characterized by declining acceleration potential and an associated neutron yield as time progresses. Therefore, if we did not get a discharge naturally, we normally terminated this phase once the potential dropped below 150 kV by forcing a discharge before initiating the cool-down process. Otherwise, the entire chamber tends to get too hot, making it impossible to subsequently cool the crystals from 130 °C down to 0 °C within 20 min. Concentrating only on the heating phase, it should be noted that after the crystal potential has declined to values below the break-down potential of the ionized gas, neutron production has been observed to continue for at least 30 min before the yield approached the natural neutron background level.

Although the current and potential are both higher during the cooling phase of the crystals then during the heating phase, the associated radiation readings are not as high as observed during the heating process. One possible explanation is the conjecture

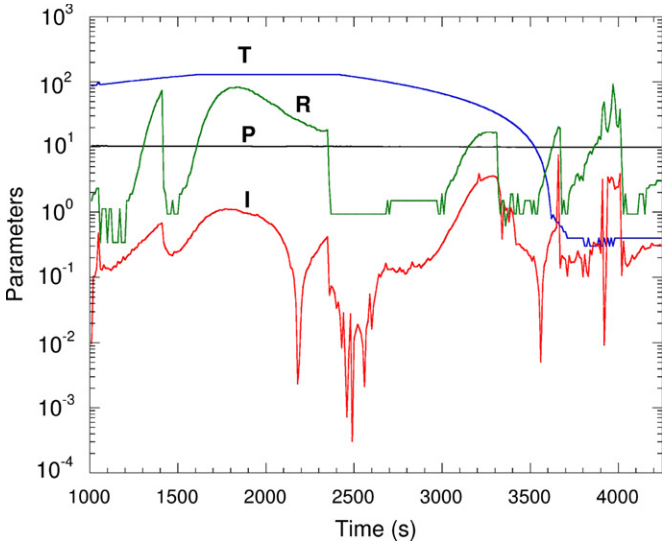

Fig. 11. Same as 10, but in this case the neutron yield during the 12-min long time interval between 1600 and 2325 s was almost a factor of five above the natural neutron background level. The first 1000 s are not shown.

that during the heating phase some of the X-ray radiation originates from electrons striking the current collecting disk (which is closer to the Geiger counter) rather than the positively charged front face of the right crystal.

The determination of the maximum electron energy during the cooling phase is not as easy and accurate as during the heating phase. Due to its location our HPGe detector does not have a direct view of the front face of the left crystal 2 which carries a positive polarization charge during cooling. Nevertheless, we have routinely recorded maximal X-ray bremsstrahlung end-point energies of about 350 keV just before discharges. Typically, we experienced three discharges during the cool-down phase, resulting in two time intervals with substantial neutron production, each lasting about 2–3 min. Due to higher potentials, these time segments are typically shorter than those observed during the heating phase. In addition, and again in contrast to the heating phase, we could not extend neutron production for a longer period of time after the crystal potential dropped considerably below the break-down potential. This is due to the fact that with the present heater/cooler device the crystal temperature could not be maintained at 0 °C for longer than about 10 min before the crystals started to warm up to room temperature, and as a result the polarization potential declined to low values, making it impossible to record neutrons above natural background levels.

Fig. 11 shows that the second neutron production phase can be quite productive. In this case only one discharge took place during the heating phase of the crystals. During the constant temperature phase neutrons were produced continuously with a net neutron yield above the background of 20 per minute during a 12-min time interval. Note again the change in current polarity during this phase. It should also be mentioned that during this run the current collecting disk was removed, and the current was collected from the insulated chamber wall, resulting in higher current readings compared to Fig. 10.

4. Tests to verify the correctness of results

Numerous tests were performed to verify the correctness of the results reported above. The most important ones are briefly described in this section.

Before evaporating deuterated polyethylene on the right crystal surface, runs were performed with "naked" crystals. These runs resulted in a small neutron yield, about 5% of the yield observed with "deuterated" crystals. These findings are consistent with neutron production in deuterium gas ("gas neutrons") [4]. Replacing the deuterium gas by regular hydrogen gas at the same pressure provided zero neutron yield above room background. Next, we evaporated deuterated polyethylene onto the face of the right crystal. Returning to deuterium gas, in this case neutrons were not observed during the heating phase of the crystals (except for the few "gas neutrons"). Only during the cooling phase did we observe a substantial amount of neutrons. It may be interesting to note that even with only one crystal "deuterated", we could not reach the maximum potentials observed with two "naked" crystals. After evaporating deuterated polyethylene on the face of the left crystal we produced substantial amounts of neutrons also in the heating phase of the crystals. The associated results were shown already in Fig. 8. Before evaporating new layers of deuterated polyethylene on the crystal surfaces, we removed the deuterated polyethylene from the left crystal in order to investigate once more if larger neutron yields could be obtained during cooling with only one crystal "deuterated". This turned out to be not the case. We also checked once more on our earlier finding that only "gas neutrons" are produced with "naked" crystals by removing the deuterated polyethylene from the right crystal surface as well. Afterward, two new layers of deuterated polyethylene were evaporated on the two crystal faces and the associated results were given in Fig. 9.

In order to compare our neutron pulse-height distribution with the spectrum reported in Ref. [8], we projected the neutron events shown inside the gate of Fig. 6 onto the pulse-height axis and added up the neutron pulse-height spectra for the runs summarized in Fig. 8. The resulting sum spectrum is shown in Fig. 12 together with the natural neutron background spectrum in the energy region of interest. The shape of this sum spectrum is consistent with our experience in this neutron energy range, but it is considerably different from the spectrum shown in [8], which shows an enhancement in yield near the center of the pulse-height distribution, which is about a factor of two higher than the yield just above threshold. The dimensions of the neutron detector used in Refs. [2,7–9] are similar to our 5-in. diameter detector, except for a thickness of 3 in., versus 2 in. in our case.

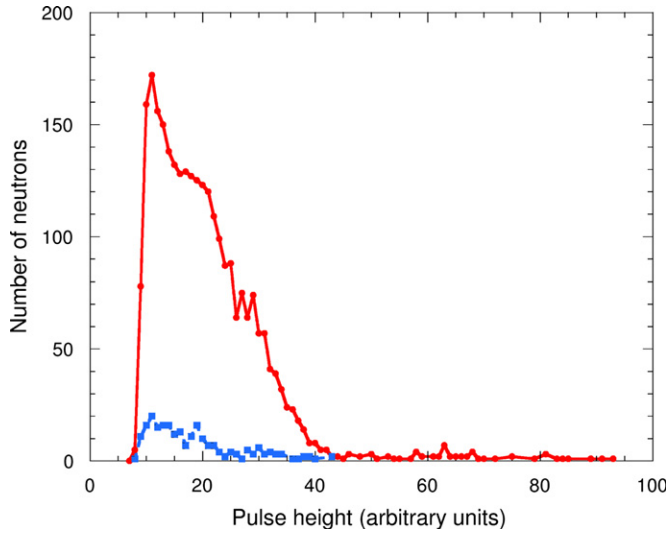

Fig. 12. Neutron detector pulse-height spectrum (dots) and natural background spectrum (squares for channel numbers below 43 and dots for channel numbers 43 and above) for the runs of 8.

This increase in thickness certainly favors double scattering in the neutron detector and results in a small enhancement at larger pulse heights. However, we are not aware of any mechanism that provides a pulse-height distribution as given in Ref. [8], assuming a reasonable light-response function and a properly working lower-level discriminator. The neutron energy spectrum of Ref. [8] is also inconsistent with the one given in Ref. [1].

In order to check on the correctness of the neutron energy spectrum shown in Fig. 12 we produced 2.5 MeV neutrons using our Low-Energy Beam Accelerator Facility (LEBAF) at TUNL to initiate the reaction ^{2}H(d,n)^{3}He with an incident 160 keV deuteron beam. Using electronics identical to those used in our pyrofusion experiments, neutron pulse-height distributions were measured for our 5- and 2-in. diameter detectors. They matched very well with the spectrum obtained in our pyrofusion runs shown in Fig. 12.

We would like to mention that we also used these ^{2}H(d,n)^{3}He studies at LEBAF to empirically determine the attenuation (7%) of our lead shields so that we could check on our Monte-Carlo calculations referred to in Section 5. To do this we took runs with and without lead shields placed around our two types of neutron detectors and normalized the yields to an independent neutron monitor detector.

5. Neutron yields

The neutron yields given in Section 3 refer to the recorded neutron yields obtained with our two 5-in. dia. $\times$ 2-in. thick and 2-in. dia. $\times$ 2-in. thick neutron detectors placed at the positions indicated in Figs. 2 and 4. The neutron detection efficiency of the detectors used in the present work is known at the 3% level, either due to direct measurements or Monte-Carlo simulations [15]. The neutron detection efficiency of a 2-in. thick liquid scintillator detector of the type Bicron 501A (or NE213) at $\frac{1}{4}$ times ^{137}Cs threshold for 2.5 MeV neutrons is 0.39 for the 5-in. diameter detectors and 0.36 for the 2-in. diameter detectors. Using these efficiencies and the neutron attenuation in the lead shields placed around the neutron detectors, the Monte-Carlo simulation of our experimental setup predicts that the maximum yield of 493 neutrons per thermal cycle found in the present work corresponds to $16\,250 \pm 1600$ neutrons generated. This yield is about 60% higher than the most recent yield reported by the RPI group in Ref. [8] using an electric-field enhancing nano-tip. However, it is about a factor of 3.7 lower than the maximal yield reported in Ref. [7] by the same group. Taking into account the considerably higher energies achieved in the present work and the fact that neutrons were produced both during the heating and cooling phases of the crystals, a substantially higher neutron yield could have been expected. Obviously, the nano-tips used in Refs. [1–3,7–9] are providing a large enhancement factor.

6. Summary

We have produced unprecedented high potentials of up to 400 kV with a pyroelectric double-crystal setup. Without using a nano-tip we obtained a modestly large neutron yield in a consistent and fairly reproducible way, which for the first time generates neutrons via the ^{2}H(d,n)^{3}He fusion reaction during both the heating and cooling phases of pyroelectric crystals. The maximal neutron yield per thermocycle was 1.6×10^{4}. However, uncontrolled discharges limit the usefulness of the present experimental setup, although, again for the first time, our setup allows for the continuous production of neutrons (above the natural background level) during the constant temperature phase over a time period of at least 30 min. Clearly, our present work should be extended to arrangements with nano-tips, although it

will remove the beauty of producing neutrons during both the heating and cooling phases of a double-crystal arrangement, and may result in less reproducible results. However, our first priority is to investigate the cause of the premature discharges which currently prevents us from extending the uninterrupted thermal cycle at high potentials to longer periods of time. We are convinced that the neutron yield can be enhanced by at least a factor of 10 by optimizing the geometry and by the admixture of certain gases to the pure deuterium gas presently used, which could result in considerably less frequent discharges. Only once this task has been successfully completed we will concentrate on the implementation of nano-tips, which, following [1,2] should result in another factor of 10 or more increase in neutron yield.

Acknowledgements

The authors acknowledge the contributions of B. Carlin, A.S. Crowell, C.R. Howell, H.J. Karwowski, G. Rich, and S.M. Shafroth to this work. One of us (S.C.) acknowledges the National Science Foundation for awarding her a REU fellowship at TUNL (NSF ID 0851813). This work was partially supported by the United States Department of Energy, Office of Nuclear Physics under Grant No. DE-FG02-97ER41033.

References

[1] B. Naranjo, J.K. Gimzewski, S. Putterman, Nature (London) 434 (2005) 1115.
[2] J. Geuther, Y. Danon, F. Saglime, Phys. Rev. Lett. 96 (2006) 054803.
[3] V. Tang, G. Meyer, J. Morse, G. Schmid, C. Spadaccini, P. Kerr, B. Rusnak, S. Sampayan, B. Naranjo, S. Putterman, Rev. Sci. Instr. 78 (12) (2007) 123504-1.
[4] W. Tornow, S.M. Shafroth, J.D. Brownridge, J. Appl. Phys. 104 (2008) 034905-1.
[5] D. Gillich, Y. Danon, J.A. Geuther, B. Maraus, B. McDermott, in: Proceedings of the ANS/ENS International Meeting Making the Renaissance Real, Washington, DC, 2007 (unpublished), p. 927.
[6] V. Tang, G. Meyer, S. Falabella, G. Guethlein, S. Sampayan, P. Kerr, B. Rusnak, J.D. Morse, J. Appl. Phys. 105 (2009) 026103.
[7] J.A. Geuther, Y. Danon, J. Appl. Phys. 90 (2007) 174103-1.
[8] D. Gillich, A. Kovanen, B. Herman, T. Fullem, Y. Danon, Nucl. Instr. and Meth. A 602 (2009) 306.
[9] D.J. Gillich, R. Teki, T.Z. Fullem, A. Kovanen, E. Blain, D.B. Chrisy, T.-M. Lu, Y. Danon, Nano Today 4 (2009) 227.
[10] 〈http://www.ni.com/dataacquisition/〉.
[11] 〈http://www.ni.com/labview/〉.
[12] W. Tornow, S. Lynam, S.M. Shafroth, J. Appl. Phys. 107 (2010) 063302.
[13] Bicron 501A Liquid Scintillator supplied by Saint-Gobin Crystals 〈www.detectors.saint-gobain.com〉.
[14] MPD-4 Pulse-Shape Discrimination Module supplied by mesytec 〈www.mesytec.com〉.
[15] D.E. Gonzalez Trotter, F. Salinas Meneses, W. Tornow, A.S. Crowell, C.R. Howell, D. Schmidt, R.L. Walter, Nucl. Instr. and Phys. Res. A 599 (2009) 234.